Electronic Supplementary Material (ESI) for Sustainable Energy & Fuels.

Supplementary information

On

Fe and W doped Bi_2MoO_6 nanoflakes: Promising material for efficient solar water splitting

Mohua Chakraborty*, Sourav Ghosh and Venkataramanan Mahalingam*

Department of Chemical Sciences, Indian Institute of Science Education and Research

(IISER), Kolkata, Mohanpur, West Bengal 741246, India.

*E-mail: mchakraborty1988@gmail.com; mvenkataramanan@yahoo.com

Experimental Details:

1. Material Synthesis.

1.1 **Chemicals:** All chemicals are analytical grade and used as received without further purification.

1.2 **Preparation of Bi_2MoO_6, Bi/Bi_2MoO_6 and Bi films:**

The Bi_2MoO_6 (BMO) films directly deposited on fluorine doped tin oxide (FTO) coated glass substrates via solvothermal method. As starting precursor bismuth(III) nitrate pentahydrate ($Bi(NO_3)_3 \cdot 5H_2O$) of 0.5 mmol, sodium molybdate dihydrate ($Na_2MoO_4 \cdot 2H_2O$) of 0.25 mmol and ethylene glycol (25 mL) were mixed together and stirred for 2h. After dissolving all precursors, 12.5 ml of the mixed solution was poured into 25 ml Teflon lined stainless steel autoclave where FTO coated glass substrate was kept as top-down face at ≈ 45^o angle with Teflon beaker wall. After growth of BMO films at 180^{o}C for 3 (3BMO), 6 (6BMO), 12 (12BMO), 18 (18BMO), 24 (24BMO) and 30 hours (30BMO), we rinsed the coated film with deionised water, ethanol and dried at 60^{o}C for several hours. Synthesis duration and ethylene glycol have played the starring role in formation of bare BMO, Bi and Bi/BMO thin films without varying precursor concentrations.

1.3 **Preparation of $Bi_2Mo_xFe_{1-x}O_6$ and $Bi_2Mo_xW_{1-x}O_6$ photoelectrodes:**

To synthesize W and Fe doped BMO photoelectrodes, sodium tungstate dihydrate ($Na_2WO_4 \cdot 2H_2O$) and iron (III) nitrate nonahydrate ($Fe(NO_3)_3 \cdot 9H_2O$) were taken as dopant precursors, respectively. The doping concentrations of dopants were varied from 1, 3, 5% by mmol and dissolved in mixed solution of Bi $(NO_3)_3 \cdot 5H_2O$ and $Na_2MoO_4 \cdot 2H_2O$ in ethylene glycol. The $Bi_2Mo_xFe_{1-x}O_6$ and $Bi_2Mo_xW_{1-x}O_6$ films have been directly deposited on FTO with solvothermal growth at 180^{o}C for 12h duration.

Characterization:

The X-ray diffraction (XRD) of the samples were characterized using (TTRAX-III difractometer (M/s Rigaku, Japan)) with monochromatic CuKα1 radiation (λ = 1.5406 Å). Field emission SEM images and EDAX were acquired on a SUPRA 55-VP instrument with patented GEMINI column technology. Prior to loading the samples into the chamber, they were coated with a thin layer of platinum in order to avoid charging effects. TEM images were acquired on a JEM 2100F field emission transmission electron microscope operating at 200 kV. The optical absorbance of samples were characterized using Parkin Elmer LAMBDA-35 UV-Vis double beam spectrophotometer. The chemical states of products were analyzed using X-ray Photoelectron Spectroscopy with ThermoFisher Scientific XPS system. Photoelectrochemical measurements were performed on CHI604D electrochemical workstation at room temperature. The light source is 300 W Xe lamp of Newport model.

Photoelectrochemical Test:

The PEC measurements were carried out in a three electrode cells containing aqueous solution of 0.1M Na_2SO_4 (pH 7) and mixture of 0.1 M Na_2SO_4 + 0.05 M Na_2SO_3 (pH 9.3) with all BMO film coated FTO glass, platinum wire and Ag/AgCl (with 3.5M KCl solution) as working electrode, counter electrode and reference electrode, respectively. The current-density vs. Voltage curve of the working electrode was obtained by the linear sweep voltammogram (LSV) with a scan rate of 5mV/s. Mott-Schottky plots were measured at a frequency of 10 kHz in the dark. Electrochemical impedance spectroscopy (EIS) were performed at open circuit potential in same set-up with frequency 10 mHz to 1 MHz. Chronoamperometry measurement were carried out at constant potential of 0.3 V with chopped light illumination.

The applied potential shown in the bottom scale of the graph (vs. Ag/AgCl) is converted into the top scale (vs.RHE) using Nearst equation:

$$E(vs.RHE) = E(vs.\,Ag/AgCl) + 0.22 + 0.059pH \qquad (1)$$

The photo conversion efficiency (PCE%) has been calculated using equation,

$$\eta(\%) = J\{(1.23 - E_{app})/I_{light}\} \times 100 \qquad (2)$$

Where, J is the photocurrent density (mA/cm^{-2}), E_{app} represents the magnitude of applied potential in V vs. RHE, and I_{light} is incident power (mW cm^{-2}).

The study of the carrier lifetime and recombination behaviour has been analyzed with the calculated transient decay time from chronoamperometry measurement according to the formula [S1]

$$\tau_D = \frac{I_t - I_{st}}{I_{in} - I_{st}};$$

where I_{in} and I_t are photocurrent density at 0 s and t s, I_{st} represents steady state current achieved when charge generation and recombination rates reached equilibrium. The transient decay time τ is defined as the time when $\ln^{\tau_D} = -1$ [S2].

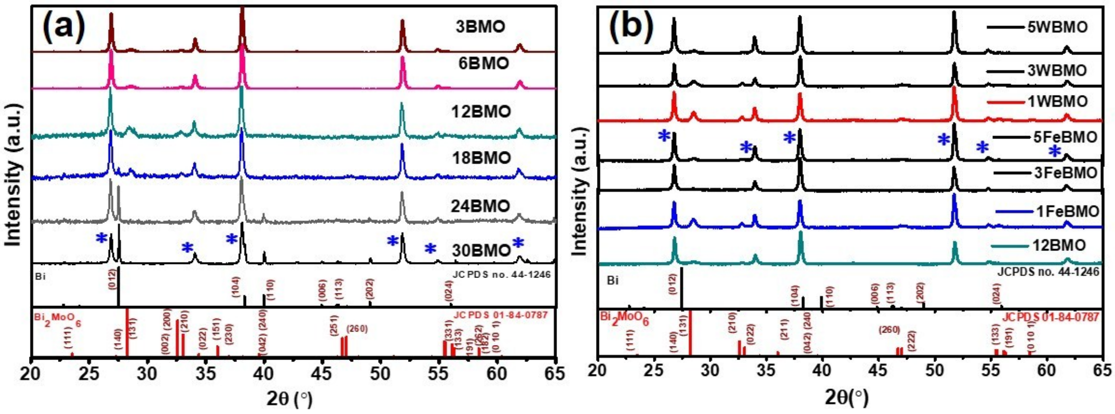

Fig. S1: XRD patterns of BMO thin films **(a)** at different synthesis duration **(b)** with different concentration of Fe and W doped.

The variation in growth duration represents the change in crystallinity and phase structure of the system. All peaks for 3BMO, 6BMO and 12BMO can be assigned to the orthorhombic structure of Bi_2MoO_6 as JCPDS card 01-84-0787 and space group PCa21. The samples 3BMO, 6BMO and 12BMO represents the high intense peaks of Bi_2MoO_6 with larger FWHM at 28.3^o (131) and 32.6^o (200) corresponds to narrow size nanoparticles. The XRD pattern for 18BMO indicates peak intensity and FWHM of (131) and (200) peaks relates to Bi_2MoO_6 reduced and new peaks started to arise at 27.4^o (012), 37.9^o (104) and 39.5^o (110) corresponds to Bi element (JCPDS card 44-1246). Whereas, further increase in growth duration to 24 and 30h represents the peak corresponds to Bi_2MoO_6 disappeared and highest intense peaks correspond to Bi elemental phase is leading.

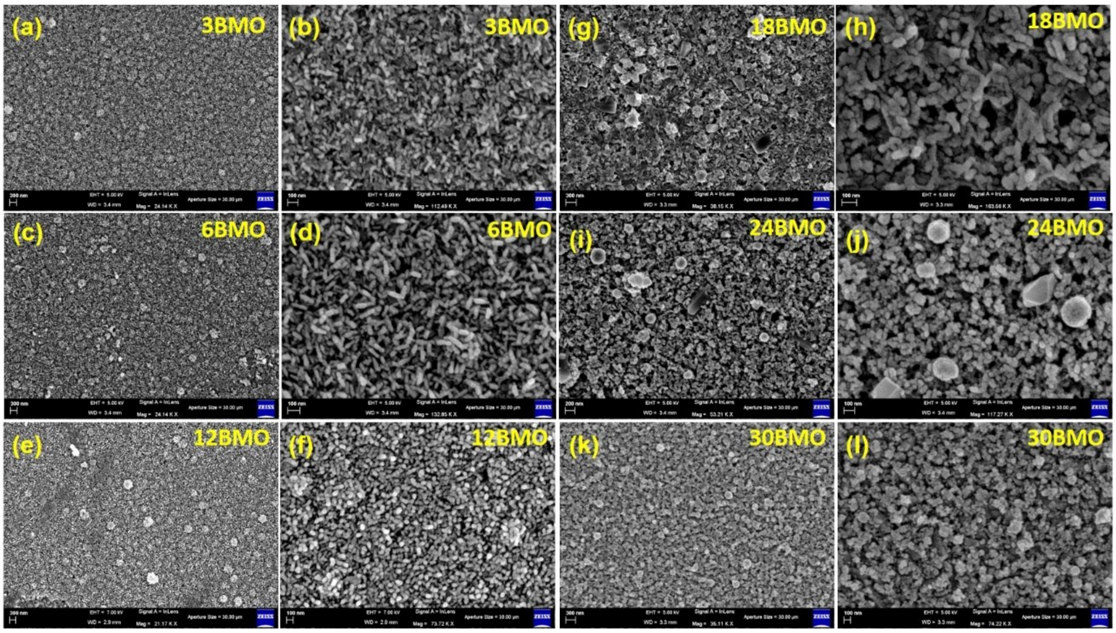

Fig. S2: Top view of the SEM images of BMO nanoflakes thin films grown on FTO coated glass for duration (a-b) 3h, (c-d) 6h, (e-f) 12h, (g-h) 18h, (i-j) 24h, (k-l) 30h.

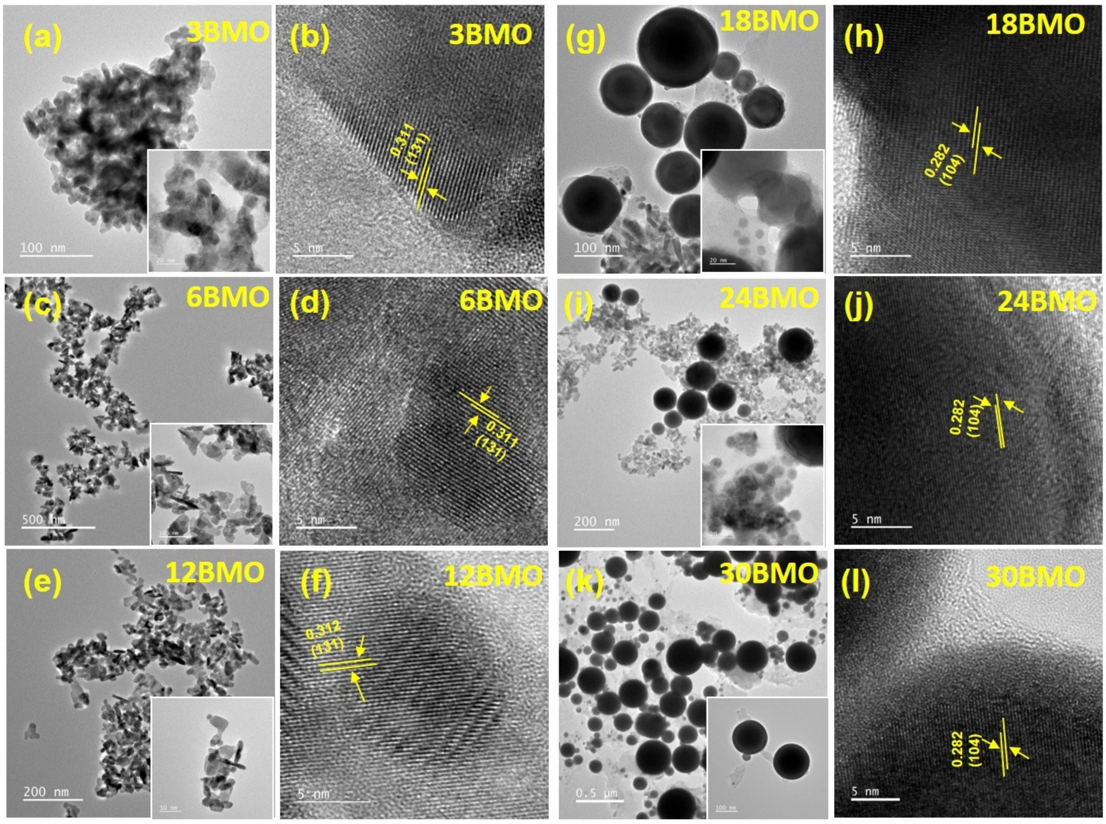

Fig. S3: TEM and HRTEM images of BMO nanoflakes grown for duration (a-b) 3h, (c-d) 6h, (e-f) 12h, (g-h) 18h, (i-j) 24h, (k-l) 30h.

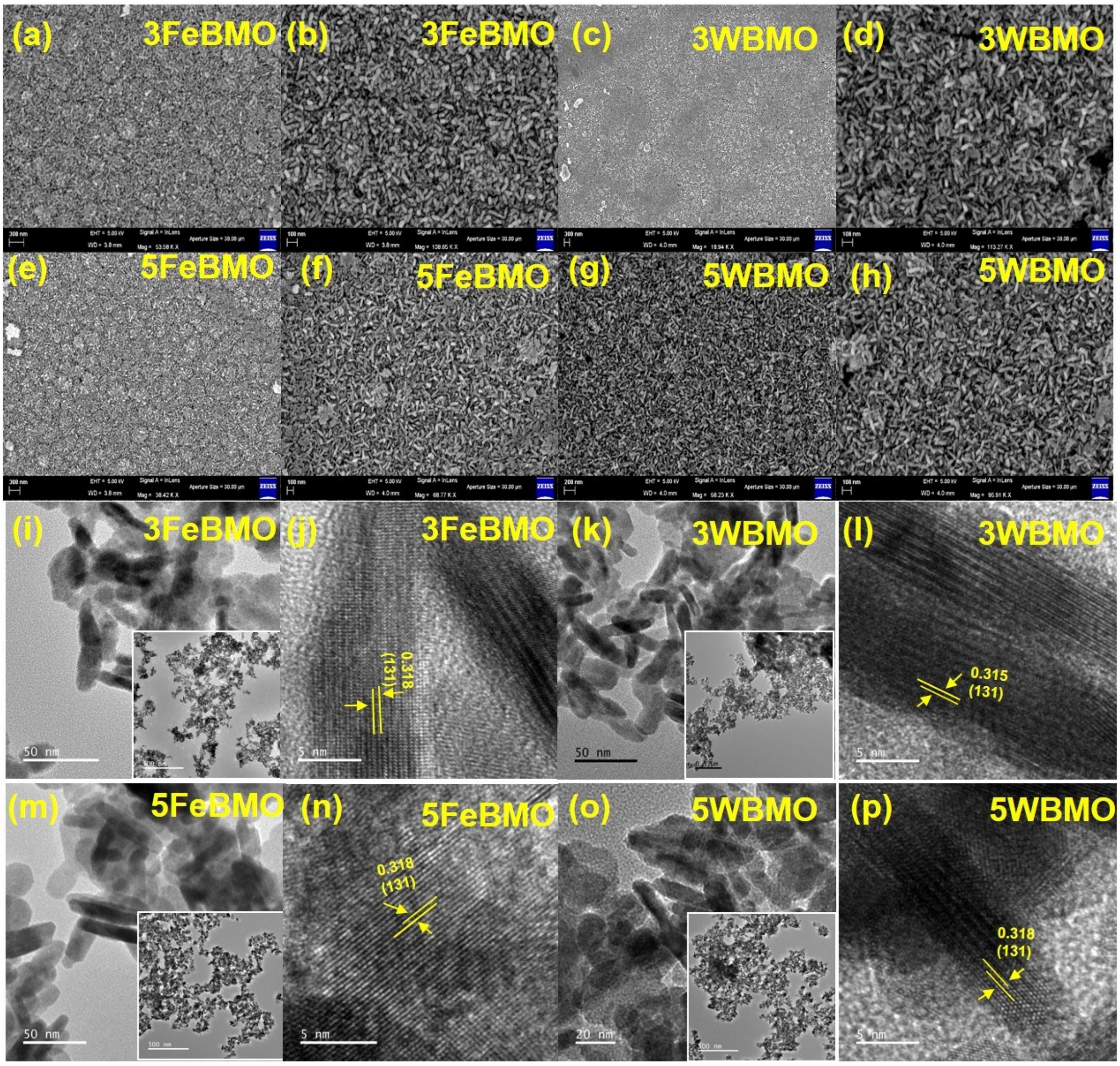

Fig. S4: SEM images of BMO nanoflakes thin films grown on FTO coated glass with dopant (a-b) 3% Fe, (c-d) 3% W, (e-f) 5% Fe, (g-h) 5% W, TEM and HRTEM images of BMO nanoflakes grown with (i-j) 3% Fe, (k-l) 3% W, (m-n) 5% Fe, (o-p) 5% W.

The whole FTO coated glass substrates for samples 3BMO, 6BMO and 12BMO are uniformly covered with vertically aligned nanoflakes of average thickness about 27 nm and the length is around 95 nm.

The increase in synthesis duration at constant temperature enlarged size of elemental Bi and helped to get separated from nanoflakes surface. Although for 18BMO, small Bi nanospheres of diameter 15 to 30 nm started to grow over BMO flakes through *in-situ* reduction reaction of Bi^{3+} to Bi^{0} [S3], which can be observed with TEM images. Further increase in synthesis duration for 24BMO; the product contains small Bi nanospheres of diameter 70 to 80 nm along with BMO nanoflakes. For 30 BMO, all nanoflakes has entirely converted to nanospheres of diameter in the range 40 to 90 nm and to minimize their surface energy, some nanospheres are agglomerated together and has formed bigger spheres of diameter ranging from 350 to 370 nm.

TEM images in Fig. S3 further demonstrate its flaky (3BMO, 6BMO, 12BMO), mixed phase of flakes with nanosphere (18BMO, 24BMO) and microspheres (30BMO) structure. The BMO flakes have been formed at 3h, 6h, 12h and then the smaller size Bi nanospheres were generated with increasing reaction time to 18h, which indicate the former nanoflakes were reduced. Further increase in reaction duration to 24h, TEM images of 18BMO and 24BMO in Fig. S3 clearly represents that flakes and spheres both morphologies are present in the product. Whereas, these images also revealed that with reaction duration reduction process continues to form smaller Bi nanoparticles and all those smaller nanoparticles reunite to larger size nanoparticles. These larger nanospheres in further reactions agglomerated to form microspheres as for image 30BMO to minimize its surface energy.

HRTEM image in Fig. S3, the lattice spacing values of 0.311 nm and 0.282 nm corresponds to (131) crystal planes of BMO and (104) plane of Bi respectively.

The FESEM and TEM images of all 3 and 5% Fe and W doped 12BMO thin films have been presented in Fig. S4 and values of interplaner spacing that crystal structure of BMO is not much influenced by the incorporation of small concentration of dopant ions.

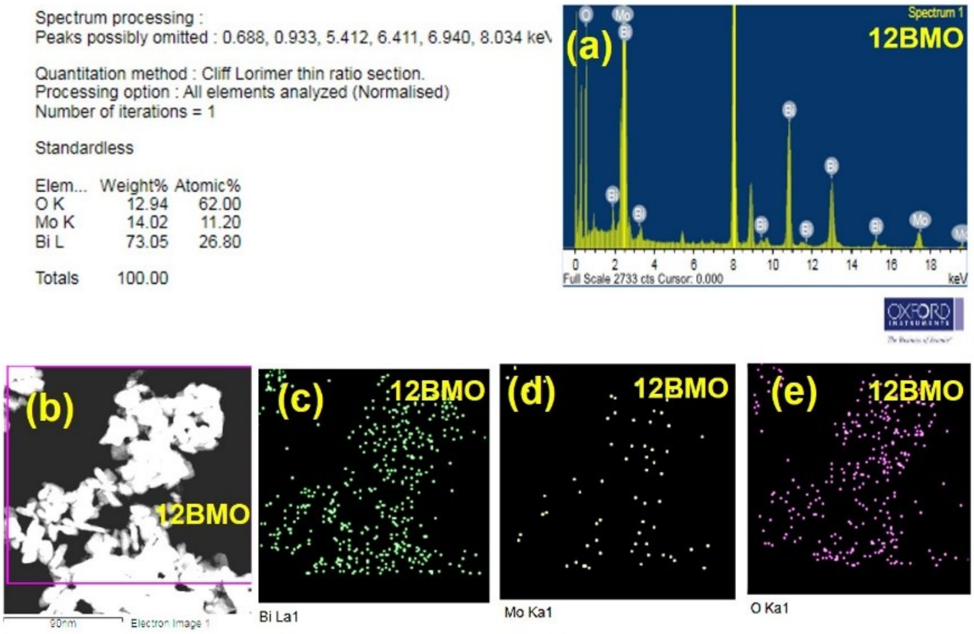

```
Spectrum processing :
Peaks possibly omitted : 0.688, 0.933, 5.412, 6.411, 6.940, 8.034 keV

Quantitation method : Cliff Lorimer thin ratio section.
Processing option : All elements analyzed (Normalised)
Number of iterations = 1

Standardless

Elem...  Weight%  Atomic%
O K        12.94    62.00
Mo K       14.02    11.20
Bi L       73.05    26.80

Totals    100.00
```

Fig. S5: Individual elemental EDAX spectra and mapping for 12BMO sample.

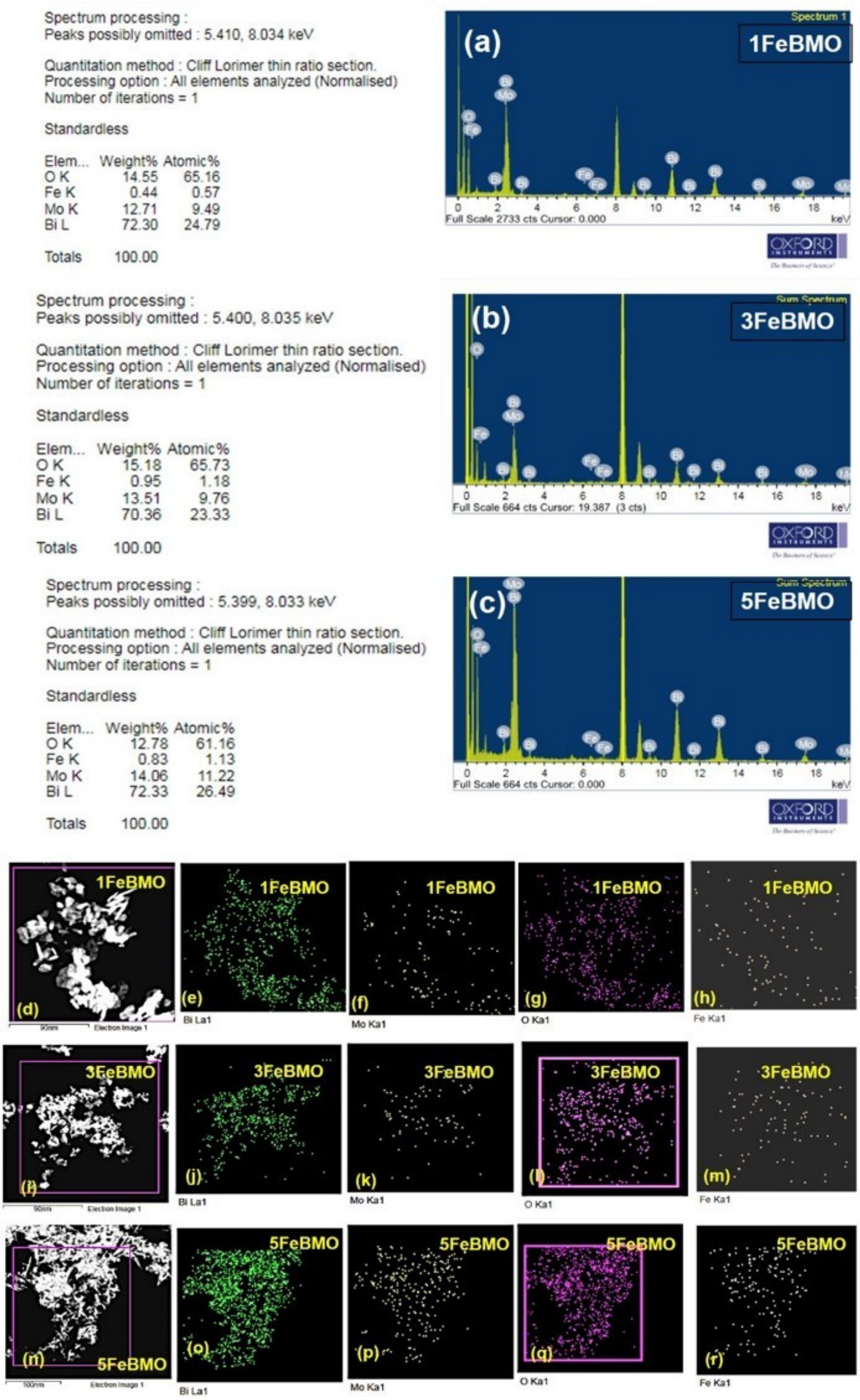

```
Spectrum processing :
Peaks possibly omitted : 5.410, 8.034 keV

Quantitation method : Cliff Lorimer thin ratio section.
Processing option : All elements analyzed (Normalised)
Number of iterations = 1

Standardless

Elem...  Weight%  Atomic%
O K        14.55    65.16
Fe K        0.44     0.57
Mo K       12.71     9.49
Bi L       72.30    24.79

Totals    100.00
```

```
Spectrum processing :
Peaks possibly omitted : 5.400, 8.035 keV

Quantitation method : Cliff Lorimer thin ratio section.
Processing option : All elements analyzed (Normalised)
Number of iterations = 1

Standardless

Elem...  Weight%  Atomic%
O K        15.18    65.73
Fe K        0.95     1.18
Mo K       13.51     9.76
Bi L       70.36    23.33

Totals    100.00
```

```
Spectrum processing :
Peaks possibly omitted : 5.399, 8.033 keV

Quantitation method : Cliff Lorimer thin ratio section.
Processing option : All elements analyzed (Normalised)
Number of iterations = 1

Standardless

Elem...  Weight%  Atomic%
O K        12.78    61.16
Fe K        0.83     1.13
Mo K       14.06    11.22
Bi L       72.33    26.49

Totals    100.00
```

Fig. S6: Individual elemental EDAX spectra and mapping for all Fe doped BMO sample.

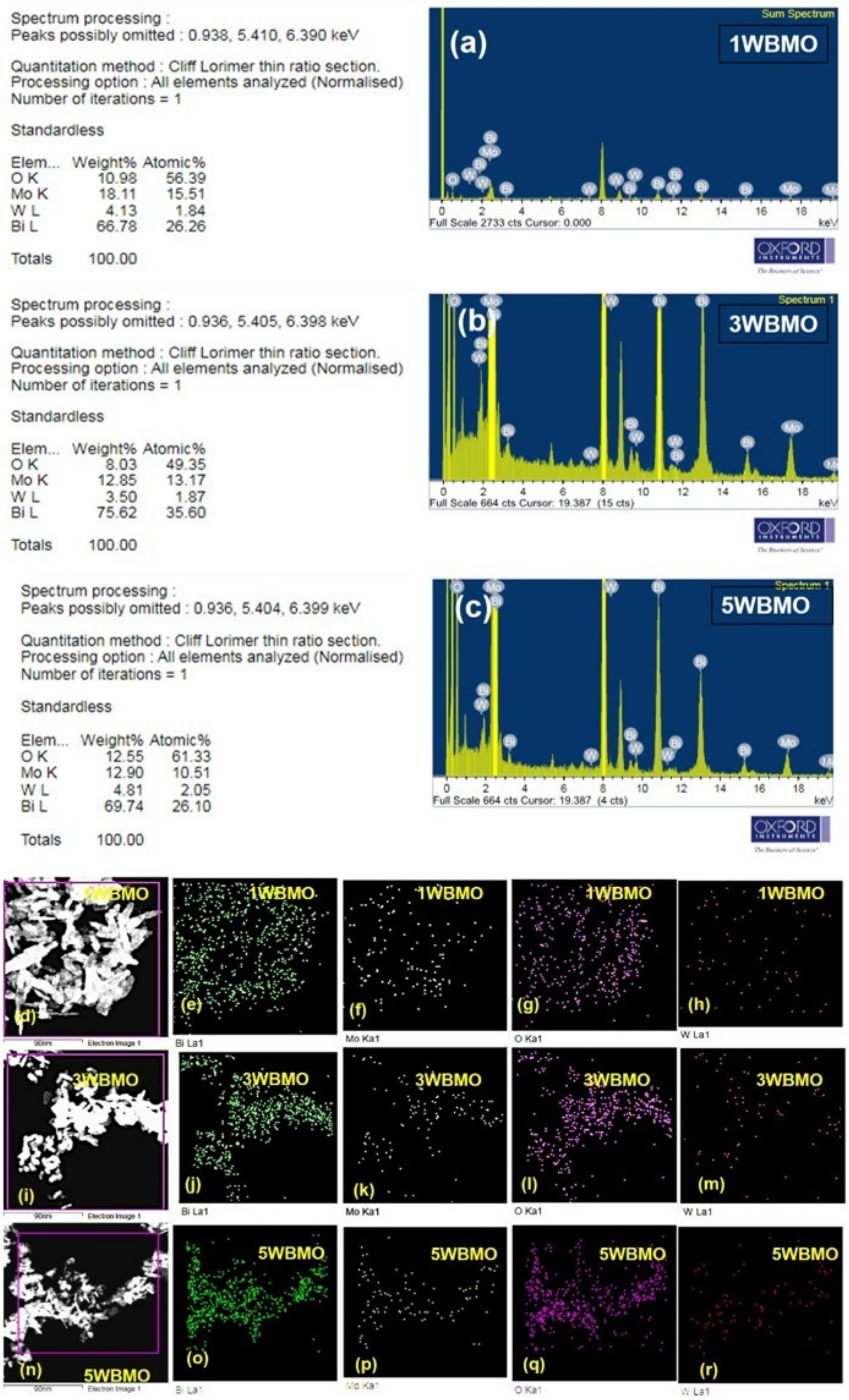

```
Spectrum processing :
Peaks possibly omitted : 0.938, 5.410, 6.390 keV

Quantitation method : Cliff Lorimer thin ratio section.
Processing option : All elements analyzed (Normalised)
Number of iterations = 1

Standardless

Elem...  Weight%  Atomic%
O K        10.98    56.39
Mo K       18.11    15.51
W L         4.13     1.84
Bi L       66.78    26.26

Totals    100.00
```

```
Spectrum processing :
Peaks possibly omitted : 0.936, 5.405, 6.398 keV

Quantitation method : Cliff Lorimer thin ratio section.
Processing option : All elements analyzed (Normalised)
Number of iterations = 1

Standardless

Elem...  Weight%  Atomic%
O K         8.03    49.35
Mo K       12.85    13.17
W L         3.50     1.87
Bi L       75.62    35.60

Totals    100.00
```

```
Spectrum processing :
Peaks possibly omitted : 0.936, 5.404, 6.399 keV

Quantitation method : Cliff Lorimer thin ratio section.
Processing option : All elements analyzed (Normalised)
Number of iterations = 1

Standardless

Elem...  Weight%  Atomic%
O K        12.55    61.33
Mo K       12.90    10.51
W L         4.81     2.05
Bi L       69.74    26.10

Totals    100.00
```

Fig. S7: Individual elemental EDAX spectra and mapping for all W doped BMO sample.

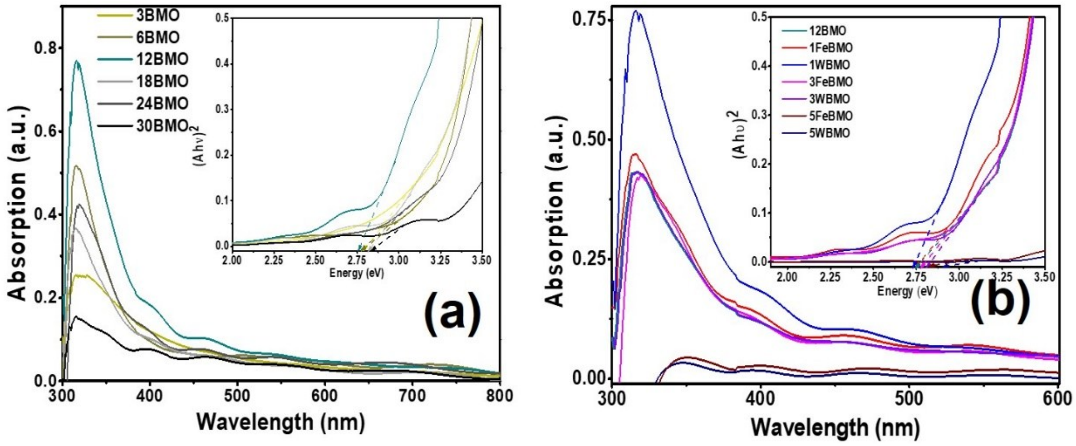

Fig. S8: UV-Vis absorption spectra for thin films grown **(a)** at different duration and **(b)** with different doping concentration of Fe and W.

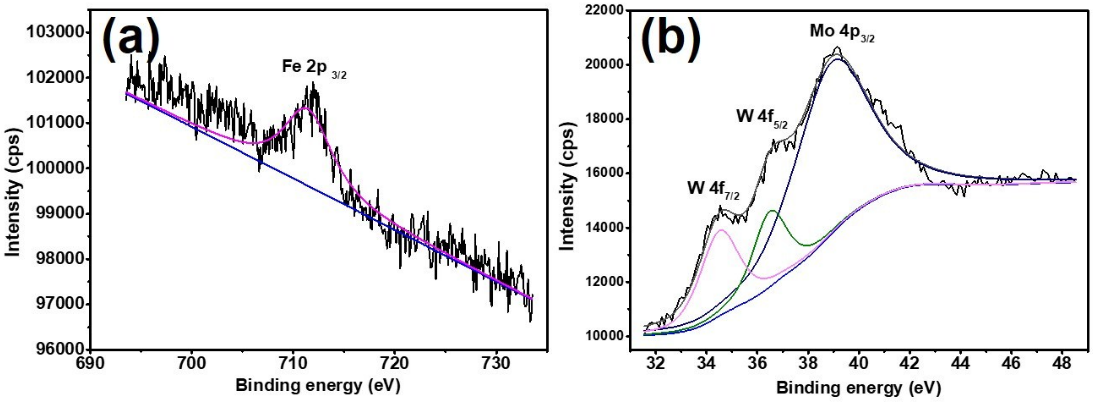

Fig. S9: XPS spectra for (a) Fe2p in 1FeBMO and (b) W 4f in 1WBMO sample.

Table S1: Atomic composition of 12BMO, 1FeBMO, 1WBMO calculated based on XPS plots shown in Fig. 5.

Sample	Peak	Raw area (cps)	Atomic percentage (%)
12BMO	Bi 4f	246000	25.6
	Mo 3d	21447	6
	O 1s	58617	68.4
1FeBMO	Bi 4f	202317	28.8
	Mo 3d	21818	8.35
	O 1s	39272	62.6
	Fe 2p	574	0.25
1WBMO	Bi 4f	279612	28
	Mo 3d	27899	7.5
	O 1s	56515	63.4
	W 4f	3888	1.05

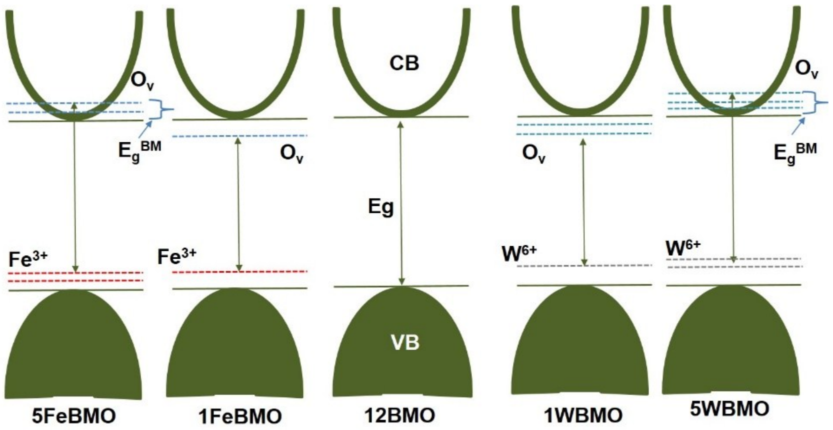

Fig. S10: Schematic diagram of the energy levels in undoped, Fe doped and W doped BMO samples.

Table S2: PEC performances of different photoanodes, photocurrent density (at 1.23 V vs. RHE) for water oxidation, photoconversion efficiency and optical band gap.

Sample	Optical band gap (eV)	Photocurrent density (μA/cm^2) at 1.23 V vs. RHE	Photo-conversion efficiency (PCE %)
3BMO	2.79	15.17	0.006% (at 0.67 V vs. RHE)
6BMO	2.77	23.16	0.005% (at 0.81 V vs. RHE)
12BMO	2.75	49.52	0.010% (at 0.83 V vs. RHE)
18BMO	2.81	17.71	0.003% (at 0.81 V vs. RHE)
24BMO	2.72	7.19	0.003% (at 0.67 V vs. RHE)
30BMO	2.83	1.73	0.0007% (at 0.67 V vs. RHE)
1FeBMO	2.74	87.39	0.021% (at 0.76V vs. RHE)
3FeBMO	2.78	61.07	0.012% (at 0.85V vs. RHE)
5FeBMO	2.83	40.25	0.012% (at 0.77V vs. RHE)
1WBMO	2.73	107.84	0.023% (at 0.86V vs. RHE)
3WBMO	2.81	51.57	0.012% (at 0.77V vs. RHE)
5WBMO	2.92	37.86	0.012% (at 0.77V vs. RHE)

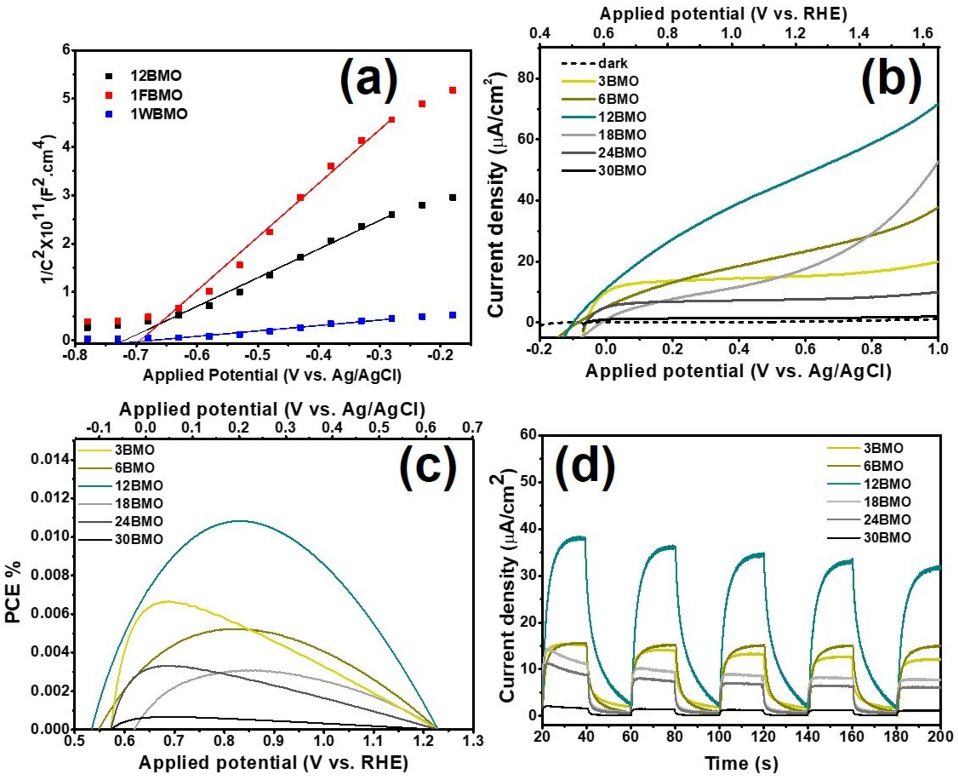

Fig. S11: (a) Mott-Schottky plots of all optimum BMO sample measured in 0.1 M Na_2SO_4 aqueous solution, **(b)** LSV curves **(c)** Photo-conversion efficiency **(d)** Chronoamperometry measurement for BMO nanoflakes grown on FTO coated glass for different synthesis duration measured in 0.1 M Na_2SO_4 aqueous solution.

Table S3: Overview of Bi_2MoO_6 photoelectrodes for photoelectrochemical application					
Morphology	**Light source**	**Scan rate (mv s^{-1})**	**Electrolyte**	**Photocurrent density**	**Refs.**
Planer and nanowall	300 W Xe lamp (50 mWcm^{-2})	10	0.5 M Na_2SO_4	18.75 and 75µAcm^{-2} @ 0.9 V$_{Ag/AgCl}$	**S4**
Nanosheet	AM 1.5G (100 mWcm^{-2})	100	0.1 M Na_2SO_4	24µAcm^{-2} @ 0.8 V$_{SCE}$	**S5**
Nanorod array	300 W Xe lamp	3	0.1 M Na_2SO_4	12µAcm^{-2} @ 0.8 V$_{SCE}$	**S6**
Nanorod array	300 W Xe lamp (100 mWcm^{-2})	100	0.2 M Na_2SO_4	4µAcm^{-2} @ 0.2 V$_{SCE}$	**S7**
Film	1000 W Xe lamp	5	0.5 M Na_2SO_4	20µAcm^{-2} @ 0.6 V$_{Ag/AgCl}$	**S8**
Film	300 W Xe lamp	5	0.1 M KCl	4.5µAcm^{-2} @ 0.6 V$_{Ag/AgCl}$	**S9**
nanoflakes	300 W Xe lamp (100 mWcm^{-2})	10	0.1 M Na_2SO_4	49.52 µAcm^{-2}@ 0.6 V$_{Ag/AgCl}$ (1.23 V$_{RHE}$)	present work
Fe and W doped nanoflakes	300 W Xe lamp (100 mWcm^{-2})	10	0.1 M Na_2SO_4	87.39 and 107.84 µAcm^{-2}@ 0.6 V$_{Ag/AgCl}$ (1.23 V$_{RHE}$)	present work

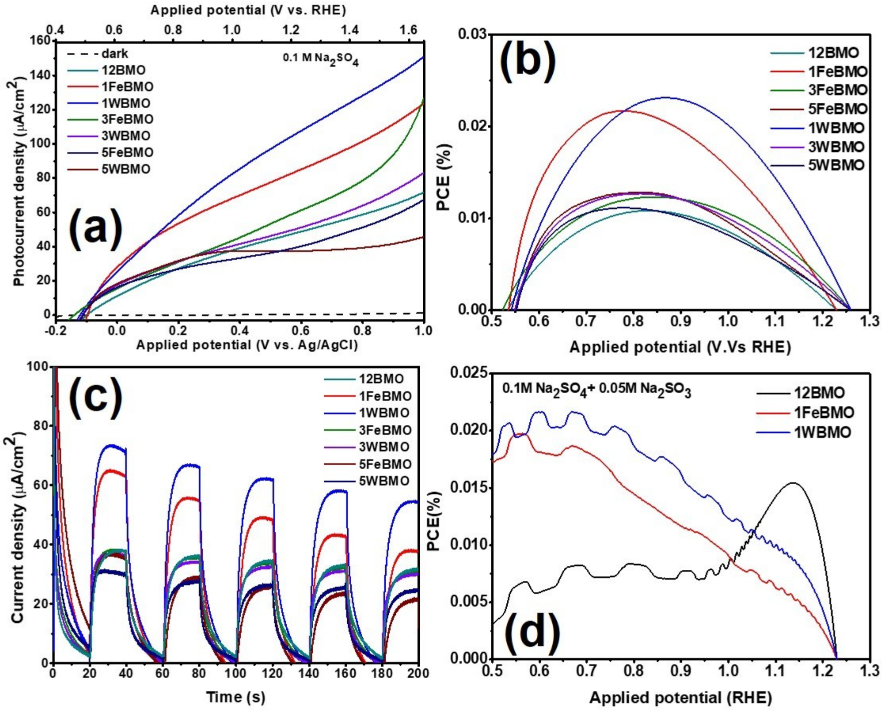

Fig. S12: (a) LSV curves **(b)** Photo-conversion efficiency **(c)** Chronoamperometry measurement for all Fe and W doped BMO nanoflakes grown on FTO coated glass for different synthesis duration measured in 0.1 M Na_2SO_4 aqueous solution, (d) Photo-conversion efficiency for all optimum sample measured in 0.1 M Na_2SO_4 aqueous solution containing 0.05 M Na_2SO_3.

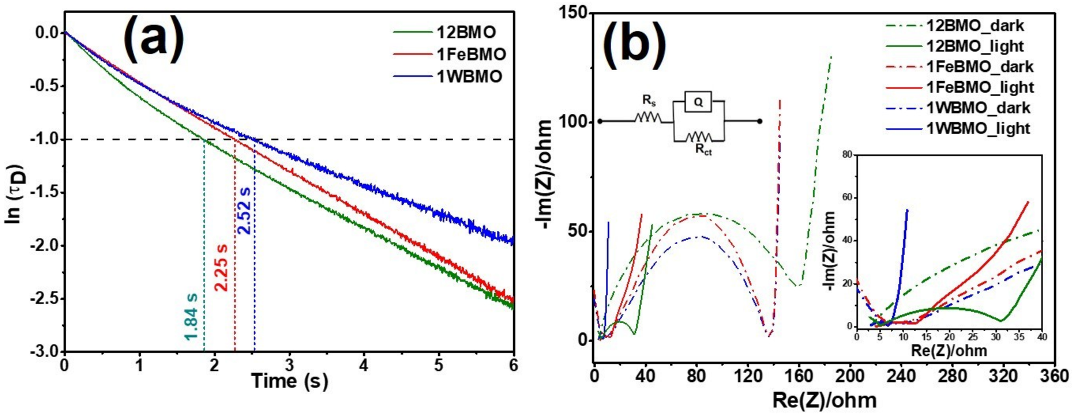

Fig. S13: (a) transient decay time and **(b)** EIS data of 12BMO, 1FeBMO and 1WBMO samples.

Table S4: Impedance parameters derived from the equivalent circuit for samples 12BMO, 1FeBMO, 1WBMO under dark and under illumination

Sample	Solution resistance R_s (Ω)	Charge transfer resistance Rct (Ω)	Constant phase element Q (10^{-10}F)
12BMO_dark	2.90	163	3.29
12BMO_light	2.87	32	2.98
1FeBMO_dar	2.30	139	2.47

k			
1FeBMO_light	**2.43**	**13**	**3.45**
1WBMO_dark	**3.57**	**138**	**6.97**
1WBMO_light	**2.43**	**7**	**4.32**

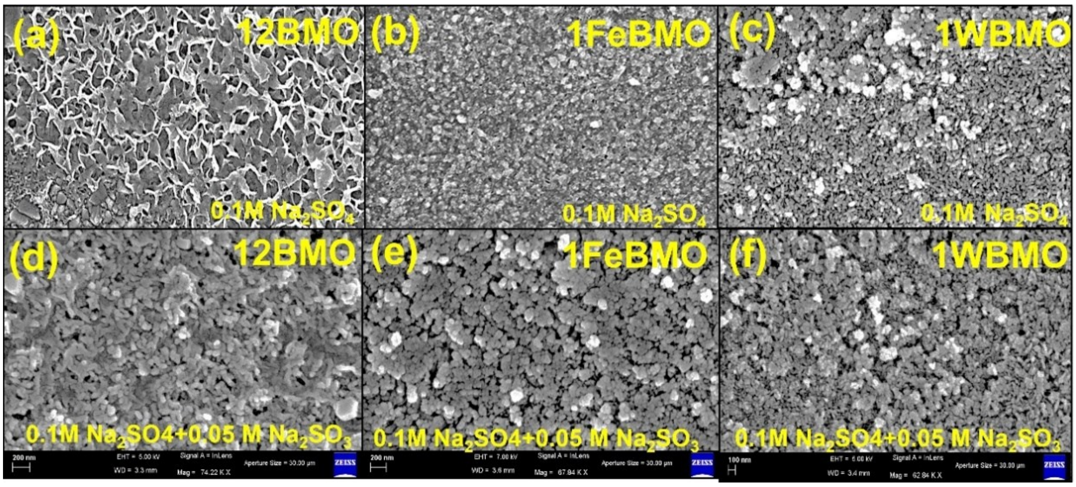

Fig. S14: SEM images measured after the 03 hours stability test of all optimum samples in (a-c) 0.1 M Na_2SO_4 and in (d-f) 0.1 M Na_2SO_4 aqueous solution containing 0.05 M Na_2SO_3.

References:

- **S1.** Y. Sun, Z. Sun, S. Gao, H. Cheng, Q. Liu, J. Piao, T. Yao, C. Wu, S. Hu, S. Wei and Y. Xie, Nat. Commun. 2012, 3 (1-7), 1057.
- **S2.** N.J. Bell, Y.H. Ng, A. Du, H. Coster, S.C. Smith, R. Amal, J. Phys. Chem. C, 2011, 115, 6004 – 6009.
- **S3.** Y. Ma, Y. Jia, L. Wang, M. Yang, Y. Bi, Y. Qi, Efficient charge separation between Bi and Bi_2MoO_6 for photoelectrochemical properties, Chem. Eur. J. 22 (2016) 5844–5848.
- **S4.** M. Wu, Y. Wang, Y. Xu, J. Ming, M. Zhou, R. Xu, Q. Fu, Y. Lei, Self-supported Bi_2MoO_6 nanowall for photoelectrochemical water splitting, ACS Appl. Mater. Interfaces. 9 (2017) 23647−23653.
- **S5.** J. Tian, P. Hao, N. Wei, H. Cui, H. Liu, 3D Bi_2MoO_6 nanosheet/Tio_2 nanobelt heterostructure: enhanced photocatalytic activities and photoelectochemistry performance, ACS Cata. *5* (8) (2015) 4530-4536.
- **S6.** Y. Ma, Y. Jia, L. Wang, M. Yang, Y. Bi, Y. Qi, Bi_2MoO_6/$BiVO_4$ heterojunction electrode with enhanced photoelectrochemical properties, *Phys. Chem. Chem. Phys. 18* (7) (2016) 5091-5094.
- **S7.** B. Jin, Z. Jiao, Y. Bi, Efficient charge separation between Bi_2MoO_6 nanosheets and ZnO nanowires for enhanced photoelectrochemical properties, J. Mater. Chem. A 3 (39) (2015) 19702-19705.

S8. M. Long, W. Cai, H. Kisch, Photoelectrochemical properties of nanocrystalline, aurivillius phase Bi_2MoO_6 film under visible light irradiation, Chem. Phys. Lett. *461* (1) (2008) 102-105.

S9. X. Zhao, T. Xu, W. Yao, Y. Zhu, Synthesis and photoelectrochemical properties of thin bismuth molybdates film with various crystal phases, Thin solid films *517* (20) (2009) 5813-5818.